Supplementary Materials for

Long-duration hippocampal sharp wave ripples improve memory

Antonio Fernández-Ruiz*, Azahara Oliva*, Eliezyer Fermino de Oliveira, Florbela Rocha-Almeida, David Tingley, György Buzsáki†

*These authors contributed equally to this work.
†Corresponding author. Email: gyorgy.buzsaki@nyumc.org

Published 14 June 2019, *Science* **364**, 1082 (2019)
DOI: 10.1126/science.aax0758

This PDF file includes:

MATERIALS AND METHODS

Surgical Procedures

Rats (adult male Long-Evans, 300-450 g, 3-6 months old) were kept in the vivarium on a 12-hour light/ dark cycle and were housed 2-3 per cage before surgery and individually after it. All experiments were approved by the Institutional Animal Care and Use Committee at New York University Medical Center.

Electrode and optic fiber implantation were performed as described previously (*31,20*). Animals were anesthetized with isoflurane anesthesia and craniotomies were performed under stereotaxic guidance. Rats (Table 1) were implanted with silicon probes to record local field potential (LFP) and spikes from the CA1 pyramidal layer (*31*). In the optogenetic experiments, custom-designed silicon probes (NeuroNexus, Ann-Arbor) were implanted in the dorsal hippocampus (4.0 antero-posterior from Bregma and 2.6 mm from the midline). The probes (1 shank with 16 sites, 4 shanks 12 sites each; 64 sites in total; Fig. 2) were mounted on custom-made micro-drives to allow their precise vertical movement after implantation. Probes were inserted above the target region and the micro-drives were attached to the skull with dental cement. Craniotomies were sealed with sterile wax. Two stainless steel screws were drilled bilaterally over the cerebellum to serve as ground and reference for the recordings. Several additional screws were driven into the skull and covered with dental cement to strengthen the implant. Finally, a copper mesh was attached to the skull with dental cement and connected to the ground screw to act as a Faraday cage, attenuating the contamination of the recordings by environmental electric noise. After post-surgery recovery, probes were moved gradually in 50 to 150 μm steps per day until the desired position was reached. The pyramidal layer of the CA1 region was identified physiologically by increased unit activity and characteristic LFP patterns (*31,32*). The identification of dendritic sublayers was achieved by the application of CSD and ICA analysis to the LFPs (*33,34,35)*.

Optogenetic Experiments

For optogenetic experiments, rats (n = 20) were injected with AAV5-CaMKIIa-hChR2(H134R)-EYFP from UNC Vector Core (a gift from Dr. Karl Deisseroth). Three injections of 150 nL each were performed along the longitudinal axis of the dorsal hippocampi, right above the CA1 pyramidal layer. After injection, craniotomies were sealed and animals recovered in the vivarium for three weeks. Following this period, a second surgical procedure for implanting optic fibers and electrodes was performed. 200 μm core multi-mode optic fibers (Thor Labs) were implanted in the same craniotomies used previously for virus injection, right above CA1 pyramidal layer. Optic fibers were directly coupled to 460 nm blue light-emitting laser diodes (PL-450, Osram) (*21,36)* also included in the head implant. One or two silicon probes were also implanted targeting also the left of both left and right dorsal CA1 regions.

For real-time SPW-R manipulation, a closed-loop system was used in order to detect ripples online and trigger light stimulation. Once a ripple was detected, small amplitude, 100-ms, light pulse was delivered simultaneously through all fibers. The intensity was manually adjusted in each animal during a test session in the home cage by gradually increasing light power until a clear ripple was evoked. To minimize broad-band artifacts at the onset of the stimulation, trapezoid pulses with a 20 ms initial ramp were used (Fig. 2). Pulses were delivered every time a ripple was detected while the animal was performing the task in the M maze. We performed two types of control stimulations. In rats implanted with silicon probes (n = 10), the same light pulse used to prolong ripples was delivered upon detecting a SPW-R but after a random delay (400-1000 ms). In another cohort of rats (n = 5) that were also injected with virus in the same way but implanted only with optic fibers, pulses of identical shape and amplitude matching an average induced ripple in all previous animals, were delivered at random intervals (mean 1

stimuli / 5s) throughout the task.

In ripple truncation experiments (n = 5 rats), the same closed-loop system was used in order to detect ripples online and trigger a strong light stimulation. Once a ripple was detected, short pulses (10ms) of large amplitude were delivered simultaneously through all fibers, often producing a population spike followed by strong feedback inhibition of CA1 pyramidal cells, similar to the effect of electrical stimulation (*16,12)*. The intensity was manually adjusted in each animal during a test session by gradually increasing light power until post-inhibition completely silenced CA1 spiking. Pulses were delivered in a closed loop manner every time a ripple was detected while the animal was performing the task.

Behavioral Recordings

After surgery, animals where handled daily and accommodated to the experimenter, recording room and cables for 1 week before the start of the experiments. Prior to the start of the experiment animals were water restricted. One or two 30 to 60-minute-long behavior sessions were conducted daily, preceded and followed by 1 to 3 hour-long sleep sessions. Data from multiple navigational tasks was pooled for the analyses, separately for memory and non-memory demanding tasks. All memory tasks had in common that a delay period was present between trials and that there was a history-dependence of rewarded decisions, factors that typically result in a hippocampus-dependent memory load. In contrast, in non-memory tasks, animals explored the mazes freely without any specific behavioral requirement for obtaining reward (except locomotion).

Non-memory tasks

- running on a linear track (190 or 240 cm long with 10-20 cm walls), where animals run back and forth on to collect water rewards at the ends (*31)*. Session is terminated when the animal is satiated, typically one hour (n = 16).

- running on a circular track (100 cm diameter), where the animal had to run in a clockwise direction (*37)*. Water rewards were delivered in a predetermined position only when the animals had performed a full clockwise run (n = 7).

- free exploration in an enclosed open field (120 cm square, 30cm walls) or open circular platform (120 cm diameter 'cheeseboard maze'), where the animals had to explore the arena seeking randomly scattered for small food pellets (n = 10).

Memory-demanding navigational tasks

- Cheeseboard Maze (120 cm diameter), where the animals (n = 9) learned to find 3 goal wells that contained water rewards. A trial was completed once the animal had retrieved all rewards and returned to the start box to collect an additional food pellet reward. The locations of the goal wells changed daily but were fixed within a session. This strategy required animals to update their memory for the new goal locations in each session but in an otherwise familiar environment. Note that between trials there was always a delay of approximately 30 seconds. A pre-probe session was run every day to assess whether the animal remembered the previous day positions. Following the learning session, a post-probe session was also conducted to examine whether the animal remembered the newly learned locations. Inclusion of data for analysis required that the animal was pretrained for a week. In addition, the rat's performance in each included session had to show a trend of learning across trials and memory performance in probe sessions was above chance levels. Sleep sessions were recorded before and after each of learning session (*8,31)*.

- In the rectangular figure-8 maze (or 'T-maze') animals (n = 6) were trained to alternate between right and left arms to collect water reward (*31)*. At the beginning of the trial rats were confined in the start box for 15 s. After the door leading to the central arm was opened, animals ran through the central arm and chose to turn right or left. If the choice was correct (opposite arm than visited in the previous trial) they would find a water reward after turning the corner of the side arm; if incorrect, the reward port would remain empty. Only sessions when animals had been trained in the task for at least one week and performed above 80% correct trials were included. The maze was placed one meter above the floor and had 160 cm length (for the central and side arms) and 134 cm width (for the lateral connecting arms)

Novel environment exploration

A subset of the animals (n = 14) recorded in both memory and non-memory tasks were also recorded in 'novelty' exploration sessions. Novelty sessions took place a different room never visited before by the animal. The 'familiar' and 'novel' rooms had different prominent distal cues. Different behavioral apparati (described above) were used during novelty sessions: linear and circular tracks, open field and cheeseboard maze. Animals were trained to run in these mazes to collect water or food reward until they were satiated, typically 30-60 minutes. Physiological properties during novel maze exploration were compared with those in the familiar sessions in the same animals. All animals were trained for multiple days in the familiar room and behavioral apparatus, that differrd from those used in novelty sessions for each animal. To include a session in the familiar group, the animal was trained in the same task in the same room for at least one week. Novelty sessions followed familiar sessions in the same animals 1 to 3 days after the last testing in the familiar situation.

- M-maze experiments

Rats (n = 20) were allowed to recover after surgery for at least one week. First, they were pre-trained to collect sugar-water reward in the linear track. Once they were used to run and obtain rewards, the recordings in the M-maze started[7]. In the M-maze, rats were rewarded with sugar-water each time they reached the end of any of the three arms in the correct task sequence (center-left-center-right-center…). The two components of the task (outbound and inbound) were evaluated separately for assessing task performance[7]. The animal was confined at the end of the central arm for 20 s after each inbound trial. Animals performed the task for 10 days. Two sessions of 30 minutes were run in the morning and afternoon, separated by 5h and preceded and followed by ~1h sleep recording sessions. Each animal in cohorts 1 to 3 had a different stimulation protocol in the AM or PM sessions: ripple prolongation, random stimulation or no stimulation (Fig. S6). The order of the protocols was alternated across days. To prevent the confounding factor of novelty in the first session of the task, animals were exposed to the maze in the 'day zero' session for 30 minutes but without delay between trials.

The position of the animal was tracked with an OptiTrack camera system (Natural Point Corp.). IR reflective markers were mounted on the animal´s head stage and imaged simultaneously by six cameras (Flex 3). Calibration across cameras allowed for a three-dimensional reconstruction of the animal´s head position and orientation (120 Hz sampling). The maze was placed one meter above the floor and had 140 cm length (for the central and side arms) and 110 cm width (for the lateral connecting arms).

cohort	animal	virus	Implant	protocol
1	Rat1	AAV5-CaMKIIa-hChR2-EYFP	2x 16-channel probes and fibers	No stim., random stim., prolongation
1	Rat2	AAV5-CaMKIIa-hChR2-EYFP	2x 16-channel probes and fibers	No stim., random stim., prolongation
1	Rat3	AAV5-CaMKIIa-hChR2-EYFP	2x 16-channel probes and fibers	No stim., random stim., prolongation
1	Rat4	AAV5-CaMKIIa-hChR2-EYFP	2x 16-channel probes and fibers	No stim., random stim., prolongation
1	Rat5	AAV5-CaMKIIa-hChR2-EYFP	2x 16-channel probes and fibers	No stim., random stim., prolongation
2	Rat6	AAV5-CaMKIIa-hChR2-EYFP	1x 64-channel probes and fibers	Random stimulation, prolongation
2	Rat7	AAV5-CaMKIIa-hChR2-EYFP	1x 64-channel probes and fibers	Random stimulation, prolongation
2	Rat8	AAV5-CaMKIIa-hChR2-EYFP	1x 64-channel probes and fibers	Random stimulation, prolongation
2	Rat9	AAV5-CaMKIIa-hChR2-EYFP	1x 64-channel probes and fibers	Random stimulation, prolongation
2	Rat10	AAV5-CaMKIIa-hChR2-EYFP	1x 64-channel probes and fibers	Random stimulation, prolongation
3	Rat11	AAV5-CaMKIIa-hChR2-EYFP	Optic fibers	Random stimulation, prolongation
3	Rat12	AAV5-CaMKIIa-hChR2-EYFP	Optic fibers	Random stimulation, prolongation
3	Rat13	AAV5-CaMKIIa-hChR2-EYFP	Optic fibers	Random stimulation, prolongation
3	Rat14	AAV5-CaMKIIa-hChR2-EYFP	Optic fibers	Random stimulation, prolongation
3	Rat15	AAV5-CaMKIIa-hChR2-EYFP	Optic fibers	Random stimulation, prolongation
4	Rat16	AAV5-CaMKIIa-hChR2-EYFP	Optic fibers	No stimulation
4	Rat17	AAV5-CaMKIIa-hChR2-EYFP	Optic fibers	No stimulation
4	Rat18	AAV5-CaMKIIa-hChR2-EYFP	Optic fibers	No stimulation
4	Rat19	AAV5-CaMKIIa-hChR2-EYFP	Optic fibers	No stimulation
4	Rat20	AAV5-CaMKIIa-hChR2-EYFP	Optic fibers	No stimulation

Table S1: Animal assignments to different protocols in the M maze experiment

Real time SPW-R detection

Three LFP channels were used for real-time SPW-R detection. For ripple detection, a channel from the middle of the CA1 pyramidal cell layer with the largest ripple amplitude was selected and filtered

between 80 and 300 Hz. For sharp wave detection, a channel from the middle of the stratum radiatum of the CA1 with the largest sharp-wave amplitude was selected and filtered between 8 and 40 Hz. For noise detection, a channel from the neocortex where no ripple activity was present was selected and filtered between 80 and 300 Hz. The root-mean square (RMS) of the three signals was then computed by a custom-made analog circuit. Signals were fed into a data acquisition interface for real-time processing of LFP by a programmable processor (Cambridge Electronic Design - CED) at 20 kHz sampling rate. Amplitude thresholds for ripple, sharp wave and noise were manually adjusted for each animal before the start of each recording session. SPW-Rs were defined as events crossing both the ripple and sharp wave thresholds in the absence of the noise signal in the neocortical site.

Tissue Processing and Immunohistochemistry

Following the termination of the experiments, animals were deeply anesthetized and perfused transcardially first with 0.9% saline solution followed by 4% paraformaldehyde solution. Brains were sectioned in 50-70 mm thick slices (Leica Vibratome) parallel with the plane of the implanted electrodes. Sections were finally washed and mounted on glass slides with fluorescence medium (Fluoroshield with DAPI - F6057, Sigma, USA). An epifluorescence microscope (Olympus Bx61VS Epifluorescence Microscope) was used to obtain high quality photos and verify both virus expression and the tracks of both optical fibers and silicon probe shanks.

QUANTIFICATION AND STATISTICAL ANALYSIS

Electrophysiological recordings were conducted using either Intan RHD2000 interface board, sampled at 30 kHz or Amplipex KJE-1001 and sampled at 20 kHz.

Spike Sorting and Unit Classification

Neuronal spikes were detected from the digitally high-pass filtered LFP (0.5–5 kHz) by a threshold crossing-based algorithm (*Spikedetekt2*). Detected spikes were automatically sorted using the masked EM algorithm for Gaussians mixtures implemented in *KlustaKwik2*, followed by manual adjustment of the clusters using *KlustaViewa* software to obtain well-isolated single units (*38)*. Multiunit or noise clusters were discarded. Putative pyramidal cells and interneurons were separated on the basis of their autocorrelograms and waveform characteristics (*18,31)*, assisted by monosynaptic excitatory and inhibitory interactions between simultaneously recorded, well-isolated units (*39)*. For animals tested in the M-maze, spike sorting was performed semi-automatically, using 'Kilosort' (https://github.com/cortex-lab/KiloSort) (*40)*, followed by manual adjustment of the waveform clusters using the software 'Phy' (https://github.com/kwikteam/phy). Same features as with KlustaViewa (autocorrelograms and waveform characteristics assisted by monosynaptic excitatory and inhibitory interactions) were used to select and characterize well-isolated units and separate them into pyramidal cell and interneuron classes.

Offline Detection of SPW-R

To detect ripples, the wide-band signal was band-pass filtered (difference-of-Gaussians; zero-lag, linear phase FIR), and instantaneous power was computed by clipping at 4 SD, rectified and low-pass filtered (*20)*. The low-pass filter cut-off was at a frequency corresponding to *p* cycles of the mean band-pass (for 80-250 Hz band-pass, the low-pass was 55 Hz). The mean and SD of baseline LFP were computed based on the power during non-REM sleep. Subsequently, the power of the non-clipped signal was computed, and all events exceeding 4 SD from the mean were detected. Events were then expanded

until the (non-clipped) power fell below 1 SD; short events (< 15 ms) were discarded. Sharp waves were detected separately using LFP from a CA1 str. radiatum channel, filtered with band-pass filter boundaries (5-40 Hz). LFP events of a minimum duration of 20 ms and maximum 400 ms exceeding 2.5 SD of the background signal were included as candidate SPWs. Only if a SPW was simultaneously detected with a ripple, a CA1 SPW-R event was retained for further analysis. SPW-R bursts were classified when more than one event was detected in a 400 ms time window. SPW-Rs were detected only during immobility and low-theta power periods. Immobility periods were defined as periods when the detected speed was < 5 cm/s for at least 1s. SPW-R doublets and triplets were detected as two or three SPW-R events, respectively, within a window of 500ms.

Ripple spike content analysis

Well-isolated putative units with at least 100 spikes in a given session were included in the analysis. For all individual units, spikes in a [-300, +300] ms peri-ripple or stimulus onset window were collected and firing rate histograms (1 ms time bin) were constructed. All histograms for the same type of units (pyramidal or interneuron) were pooled. The firing rate histograms were z-scored and smoothed using a Gaussian kernel (SD = 5 ms). Only spikes within the interval of the detected ripples were considered for the ripple content analysis. In-ripple firing rate was calculated as number of spikes divided by ripple duration and averaged for all events. The probability of participation of individual units in ripples was defined as the number of events in which a neuron fired at least one spike during the ripple divided by the total number of ripples detected. Rank order in a given ripple was defined as the normalized temporal position (from 0 to 1) of a neuron in the sequence of all cells that participated in that ripple. The ranks were averaged for all events in which a cell participated to obtain a mean rank order. For the comparison of spikes in the early and late parts of spontaneous ripples, and randomly induced ripples were divided in two equal halves. Closed loop-prolonged ripples were divided in the spontaneous initial part, from the onset of the detected ripple to 10 ms after the onset of the light pulse (the rising phase), and in a late part (the remaining 90 ms of the pulse). Cross-correlograms were constructed with within-ripples spikes as a function of the latency binning them into 5 ms size bins. Spike counts in CCGs of all pairs in each category were z-scored, summed up, and then smoothed using a Gaussian kernel (SD = 5 ms). For peri-ripple firing histograms, single unit firing rates were z-scored and plotted as ± standard error of the mean (SEM).

Place cell analysis

Spiking data were binned into 5-cm wide segments of the place field projected back onto the maze floor, generating the raw maps of spike number and occupancy probability. Rate maps were calculated for each running direction separately (inbound and outbound travels). A Gaussian kernel (SD = 5 cm) was applied to both raw maps of spike and occupancy, and a smoothed rate map was constructed by dividing the smoothed spike map by the smoothed occupancy map. A place field was defined as a continuous region, of at least 15 cm, where the firing rate was above 10% of the peak rate in the maze, the peak firing rate was > 2 Hz and the spatial coherence was > 0.7. Place fields with fewer than 50 spikes and truncated fields were discarded (*31*). To relate the spike content of ripples to place fields on the M-maze, only pyramidal cells with single place fields in either the central or side arms, or the left or right side arms were considered.

Statistical Analyses

All statistical analyses were performed with MATLAB functions or custom-made scripts. No specific analysis to estimate minimal population sample or group size was used, but the number of animals, sessions, recorded cells and SPW-R events were larger or similar to those employed in previous

related works (*7,11,27,20,21,31)*. The unit of analysis was typically identified single cells or SPW-R events. In some cases, the unit of analysis was sessions or animals, and this is stated in the text. For rank order calculation, the probability of participation and firing rate correlations, the unit of analysis was single cells. Unless otherwise noted, for all tests, non-parametric two-tailed Wilcoxon rank-sum (equivalent to Mann-Whitney U-test), Wilcoxon signed-rank or Kruskal-Wallis one-way analysis of variance were used. For statistical comparison of behavioral and physiological parameters across stimulation conditions, 2-way repeated measures ANOVAs (main factor of group and repeated factor of day) was employed. For multiple comparisons, Tukey's honesty post-hoc test was employed. Statistical significance for main factor was reported in the main text and for post-hoc tests in figure legend. On box plots, the central mark indicates the median, bottom and top edges of the box indicate the 25th and 75th percentiles, respectively, and whiskers extend to the most extreme data points not considered outliers. Outliers are not displayed but were included in statistical analysis. Due to experimental design constraints, the experimenter was not blind to the manipulation performed during the experiment (i.e., optogenetic manipulation).

DATA AND SOFTWARE AVAILABILITY

Part of the dataset included in this study is already available in the CRCNS.org and in the buzsakilab.com databases. The rest is currently under preparation to be deposited in the same databases but will be immediately available upon reasonable request.

Custom Matlab scripts can be downloaded from https://github.com/buzskilab/buzcode.

Supplementary Figures

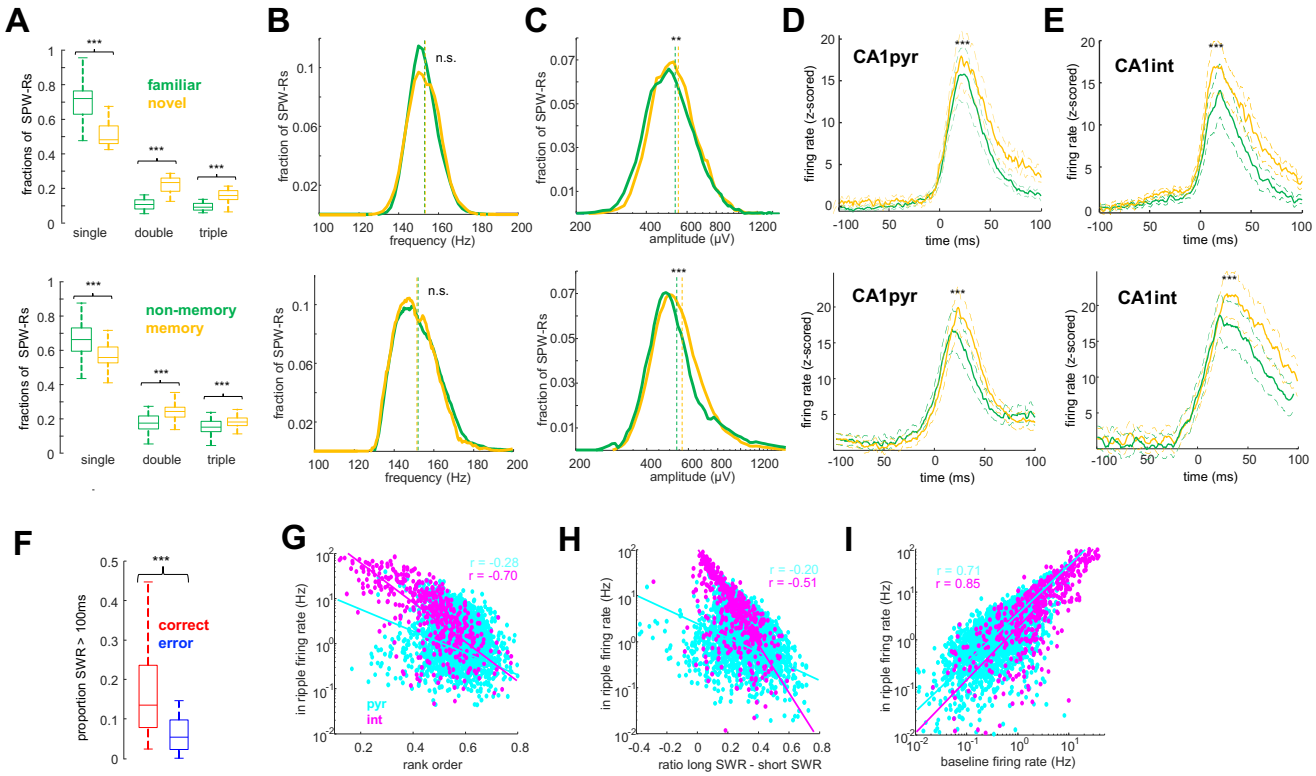

Fig. S1. Properties of SPW-Rs during different navigational tasks

(A-C). Different properties of SPW-Rs in novel or familiar environments (upper row; n = 16,732 short and 7,495 long SPW-Rs, respectively from 14 rats) and in memory or non-memory tasks (lower row; n = 33,690 and 31,637 SPW-Rs, respectively from 31 rats). (**A),** Fraction of SPW-R occurring in isolation or as doublets or triplets (in a 300-ms window). (**B**), Distribution of peak SPW-R frequencies. (**C**) Distribution of peak SPW-R amplitudes. **(D-E),** z-scored discharge firing rate patterns of CA1 pyramidal cell **(D)** and interneuron (**E**) z-scored firing rates during SPW-Rs in familiar or novel environments (upper row; n = 548/ 310 pyramidals and 93/ 71 interneurons in 11 rats) and in memory or non-memory tasks (lower row; n = 1817/ 953 pyramidals and 259/ 178 interneurons in 19 rats). *** P < 0.001, rank-sum test. **(F)**, Proportion of SPW-Rs longer than 100 ms of all SPW-Rs in the delay box of the M maze prior to correct or error trials ($P < 10^{-3}$, rank-sum test, n = 45 sessions from 10 rats) **(G)**, Correlation between within-SPW-R firing rate and the mean rank order of firing during SPW-Rs for CA1 pyramidal cells (pyr, n = 3080; R = – 0.34; $P < 10^{-79}$) and interneurons (pyr, n = 508; R = – 0.56; $P < 10^{-38}$). Note that faster firing neurons discharge earlier in SPW-R. **(H)**, Within-SPW-R firing rate as a function of that neuron's probability of firing in long versus short SPW-Rs for pyramidal cells (R = – 0.35; $P < 10^{-100}$) and interneurons (R = – 0.81; $P < 10^{-79}$). Note that slower firing rate neurons tend to occur in longer SPW-Rs. **(I)**, Correlation between within-SPW-R and baseline firing rate for pyramidal cells (R = 0.71; $P < 10^{-100}$) and interneurons. (R = 0.85; $P < 10^{-100}$). Baseline rates were calculated from the entire sleep-wake recording session

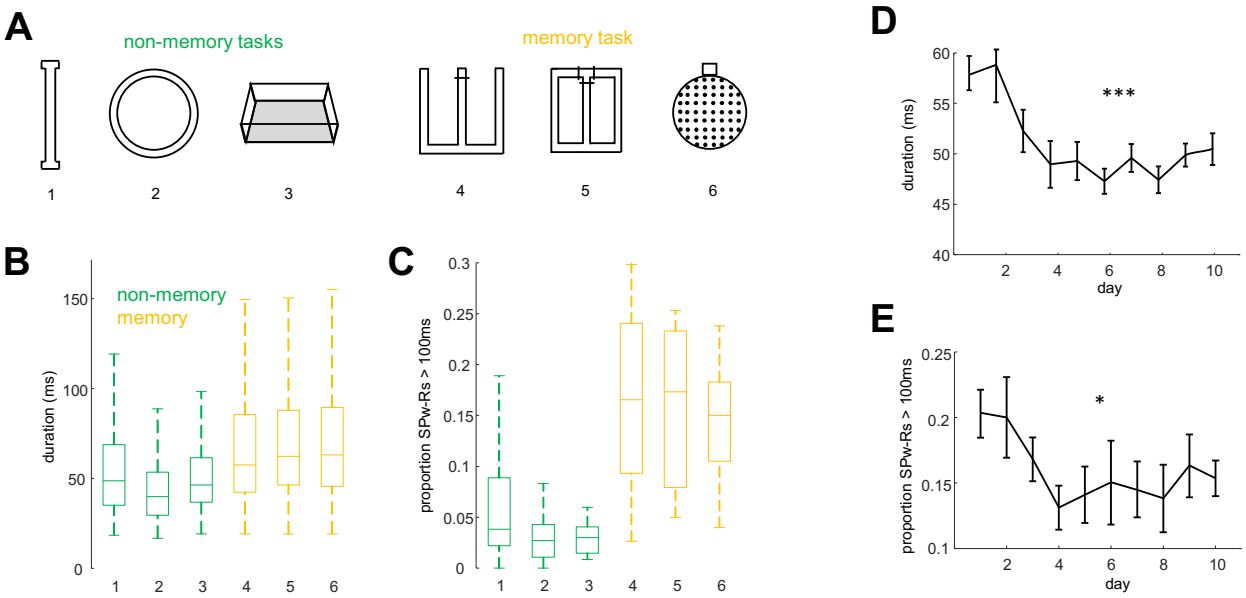

Fig. S2: SPW-R duration in individual tasks

(A), Diagrams of the different behavioral apparati used: 1- linear track, 2- circular track, 3- open field, 4- M-maze, 5- figure-8 maze, 6- cheesboard maze. (**B-C)**, SPW-R duration and proportion of SPW-Rs longer than 100 ms in the different non-memory and memory tasks. Data shown here separately for each maze was combined to generate Figure 1C. (**D-E)**, SPW-R duration and proportion of long SPW-Rs across learning days in the M-maze task (median ± standard error are shown). */*** P < 0.05/0.001 Kruskall-Wallis test.

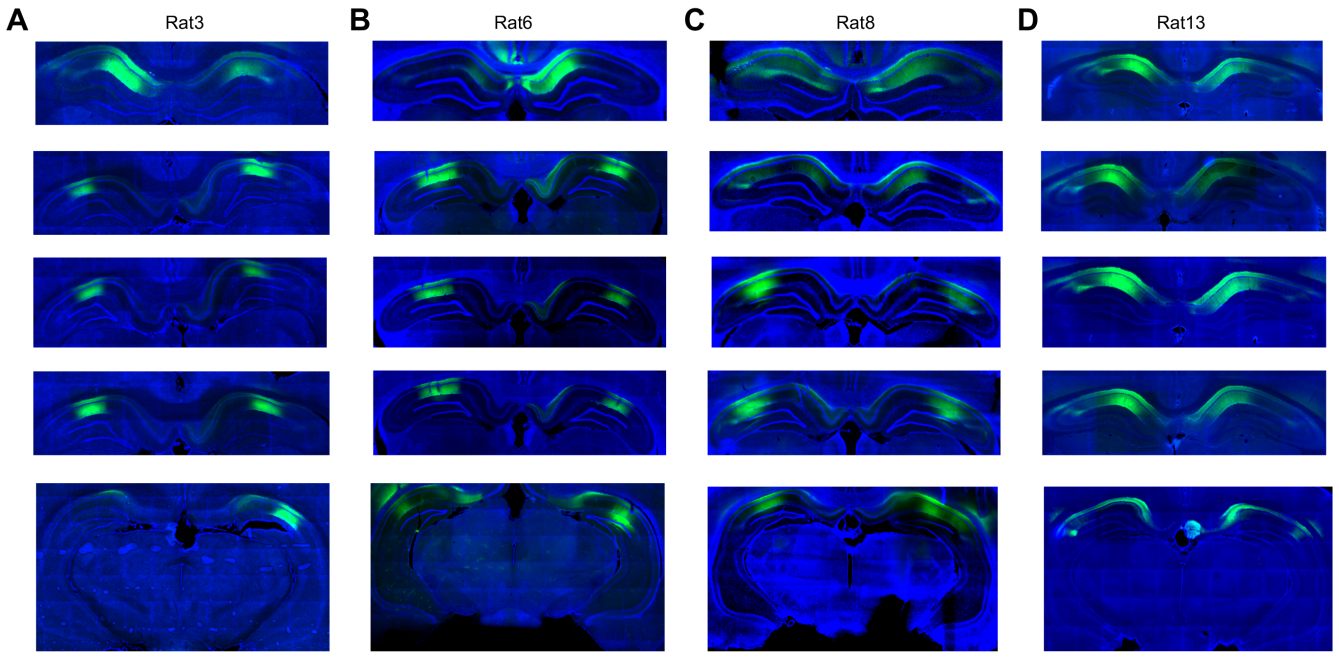

Fig. S3. Histological verification of virus expression and optic fiber and electrode placements. (A-D), Septo-temporal extent of ChR expression in four representative animals**.** Blue is DAPI staining and green ChR2-EYPF. Orange bar: 1 mm.

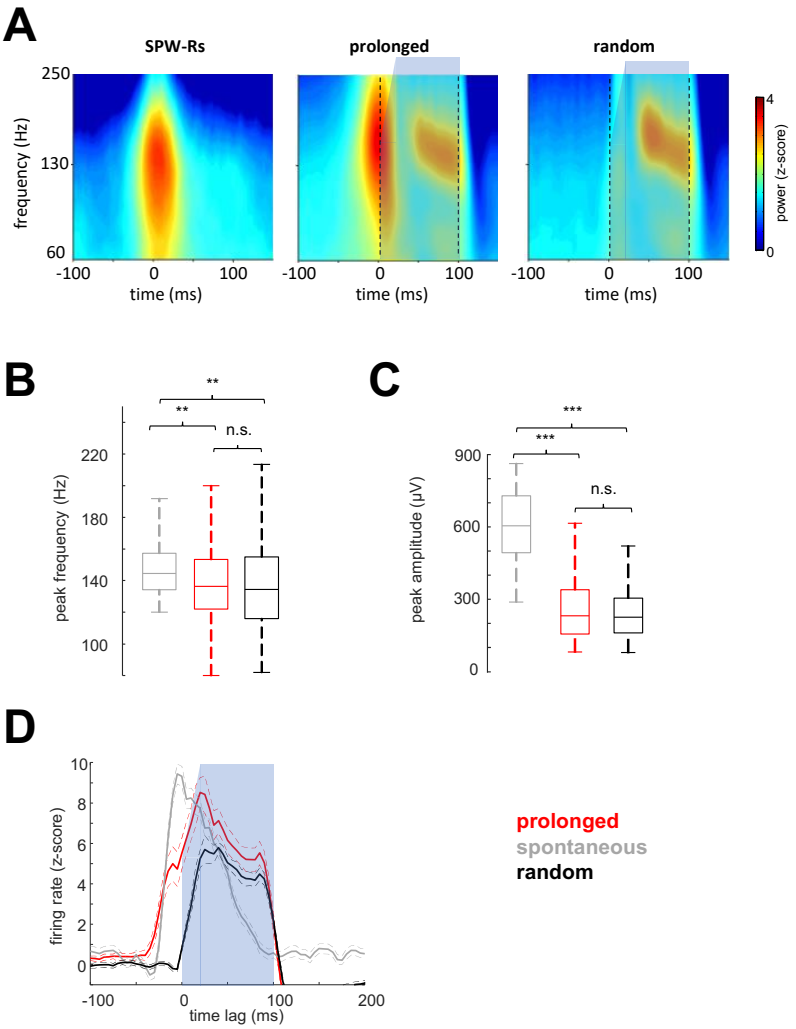

Fig. S4. Properties of artificial ripples.
(A), Averaged wavelet spectrograms for spontaneous, closed loop-prolonged and random ripples. Black dashed lines indicate blue light stimulation pulse. Blue shapes above spectrograms: waveform for optogenetic stimulation. 0 ms, onset of stimulation. Peak amplitude (**B**) and frequency (**C**) of spontaneous, prolonged and random ripples. **/*** $p < 0.01/0.001$, rank-sum test. **(D)**, z-scored firing rates of interneurons during spontaneous and induced ripples (n = 236 for closed-loop stimulation and spontaneous ripples and n = 156 for delayed stimulation from 5 rats; $P < 10^{-7}$ spontaneous versus prolonged; $P < 10^{-3}$ spontaneous versus random). 0 ms, onset of stimulation or peak of ripple power.

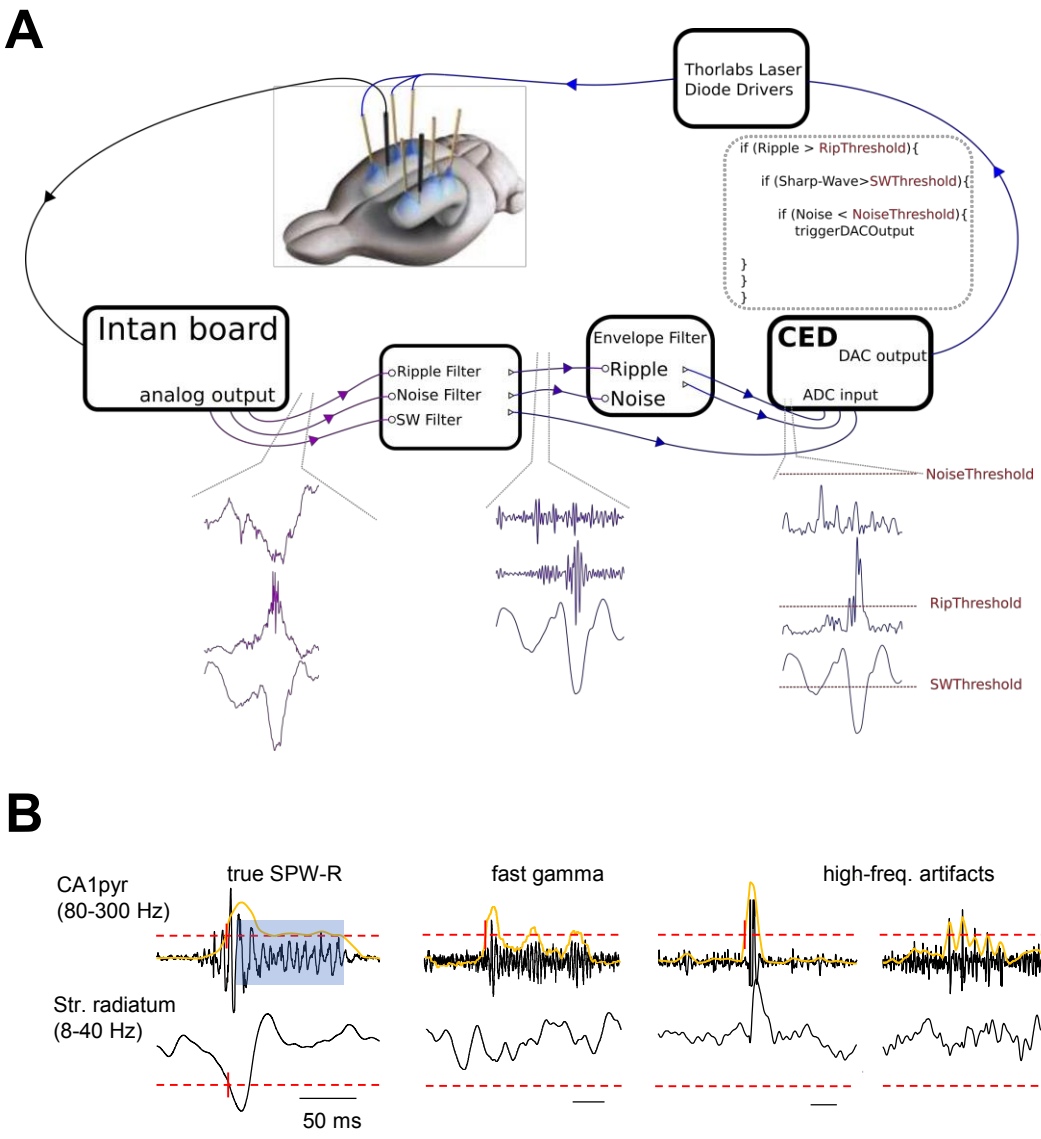

Fig. S5: Closed-loop optogenetic induction of ripples.
(A), Diagram of the system. The amplified signals are high-pass (80-300 Hz) and low-pass (8-40 Hz) filtered traces, illustrating the separation of the sharp wave and ripple. The channel with the largest amplitude ripple is rectified. Both the rectified ripple power and sharp wave are thresholded. Physiological SPW-Rs are identified by the co-occurrence of both SPW and ripple. **(B)**, Example of a prolonged ripple event. Note that the first part of the ripple is associated with a slow sharp wave component in the stratum radiatum, whereas the optogenetically prolonged ripple is not (first plot). Blue rectangle, light pulse stimulation. The other three examples illustrate false ripple detection, including fast gamma oscillation (second plot) and muscular or chewing artifacts (last two plots). These letter events are not considered true ripple events because they are not associated with a sharp-wave component. Red dashed lines show detection thresholds; yellow curves, envelops of rectified high-frequency power.

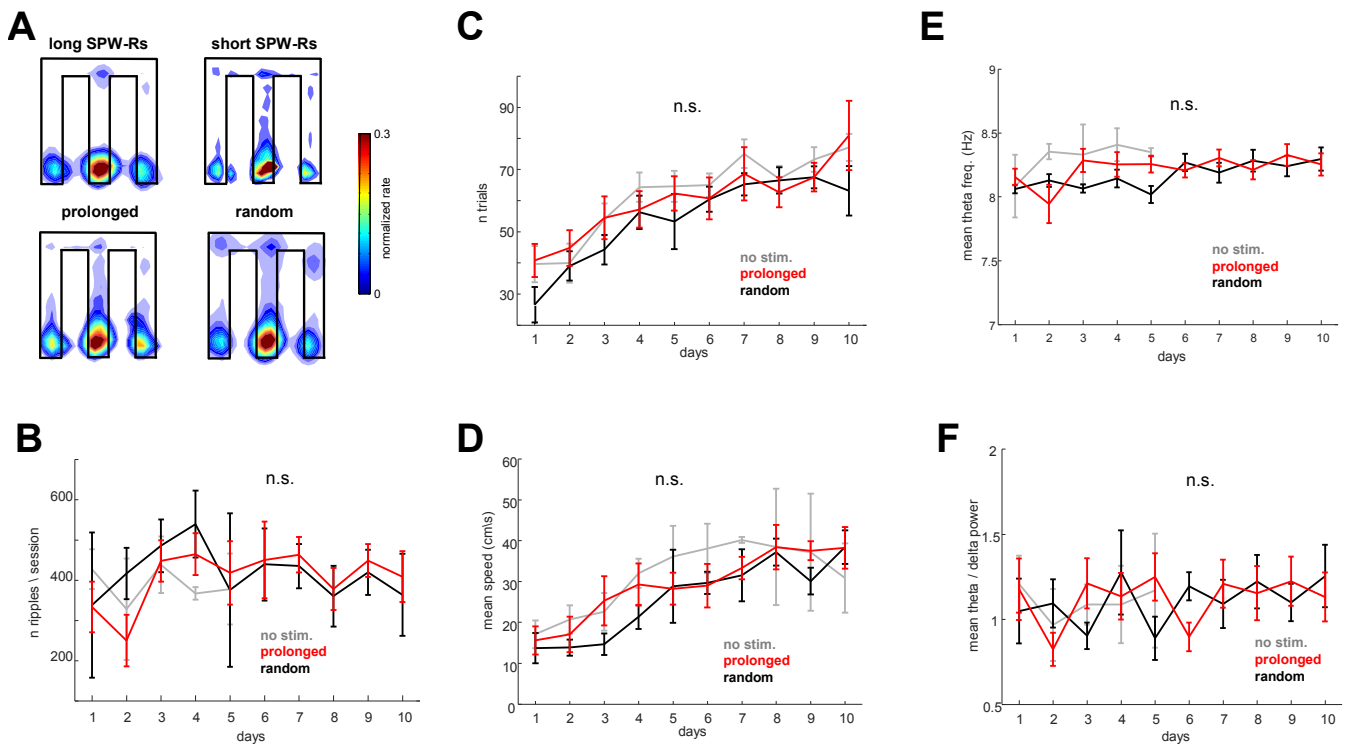

Fig. S6: Behavioral and physiological parameters of ripples during M-maze sessions.
(A), Distribution of long and short SPW-Rs, prolonged and randomly induced ripple occurrences in the M maze (n = 4,976/ 28,203/ 32,577 / 22,113 ripples from 10 rats). Number of spontaneous ripples (**B**), number of trials per 30 min sessions (**C**), mean running speed in the maze (**D**), mean theta frequency (**E**) and mean theta/delta power ratio (**F**) in no stimulation, closed-loop ripple prolongation and random stimulation sessions (n = 10 rats). (n.s. P > 0.05, repeated measures ANOVA, main effect of group)

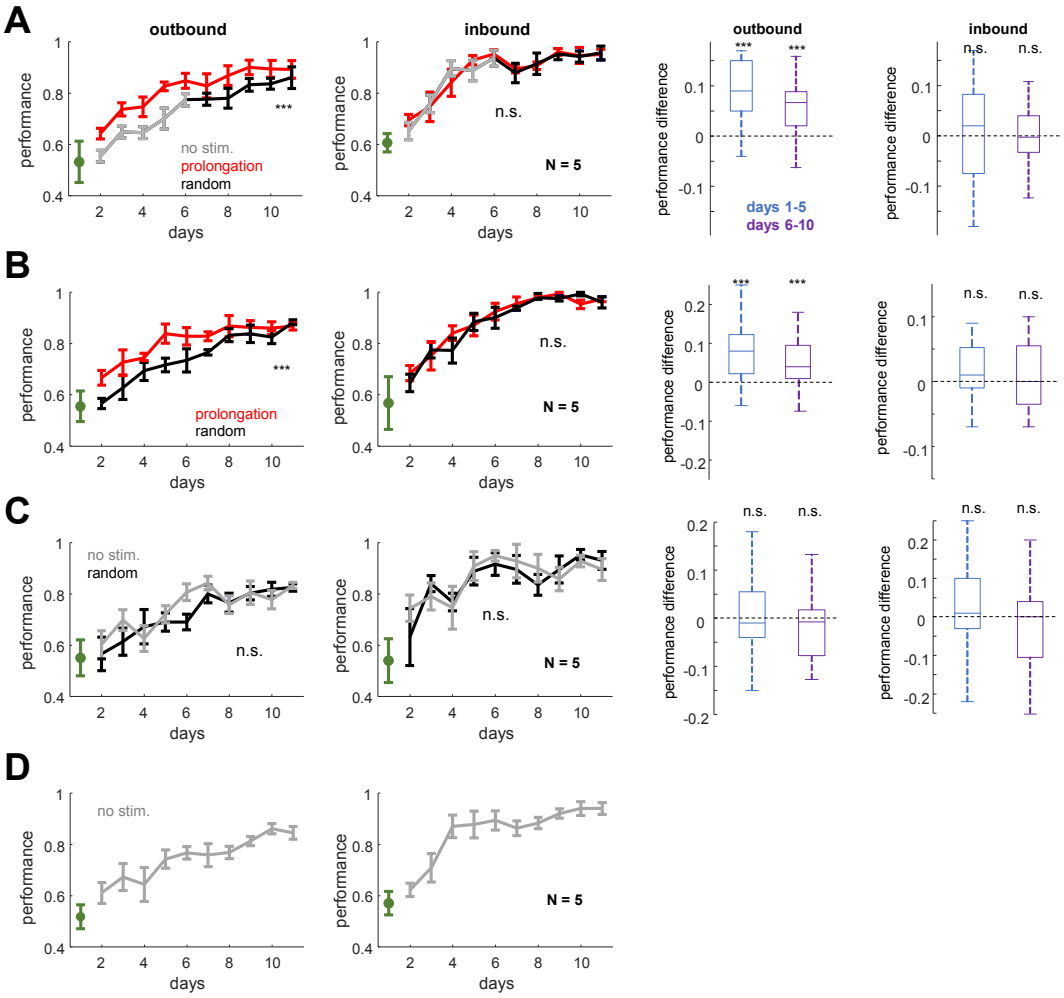

Fig. S7: Behavioral performance for the different cohorts.
Performance in the M-maze task is shown as fraction of correct trials (mean ± SEM) during outbound (first column) and inbound (second column) runs in no stimulation (grey), ripple prolongation (red) and random stimulation (black) sessions. On day 0 (green) animals had one single session without delay in the start box to familiarize with the maze. Right side boxplots: performance differences for the same day and animal for each of two conditions on a day were calculated separately for days 1 to 5 and 6 to 10 during outbound and inbound runs for all animals in each cohort. **(A)**, In this cohort, rats (n = 5) had either no stimulation or ripple prolongation sessions during the first 5 days. In days 6 to 10 they received ripple prolongation and random stimulation sessions. The types of experimental manipulations varied randomly between the morning and afternoon sessions and across animals. Main effect of group $P < 10^{-6}$ for outbound and $P > 0.05$ for inbound trials, repeated measures ANOVA. **(B)**, In the second cohort, animals (n = 5) experienced either ripple prolongation or random stimulation during the 10 days of the experiment. $P < 10^{-3}$ for outbound and $P > 0.05$ for inbound trials. **(C)**, Animals in the third cohort (n = 5) received the same virus injection as the first two cohorts and were also implanted with optic fibers but not with recording electrodes. No stimulation sessions alternated with random stimulation (one stimulation every 5s on average, 300 to 400 per session; $P < 0.05$). Light power was the same as the average used in the first two cohorts. $P > 0.05$ for outbound and inbound trials. **(D)**, Rats (n = 5) in the fourth cohort were also injected with virus and implanted with optic fibers, connected to the cable during maze behavior but received no stimulation. *** in boxplots indicate $p < 0.001$ two-sided Wilcoxon signed rank test.

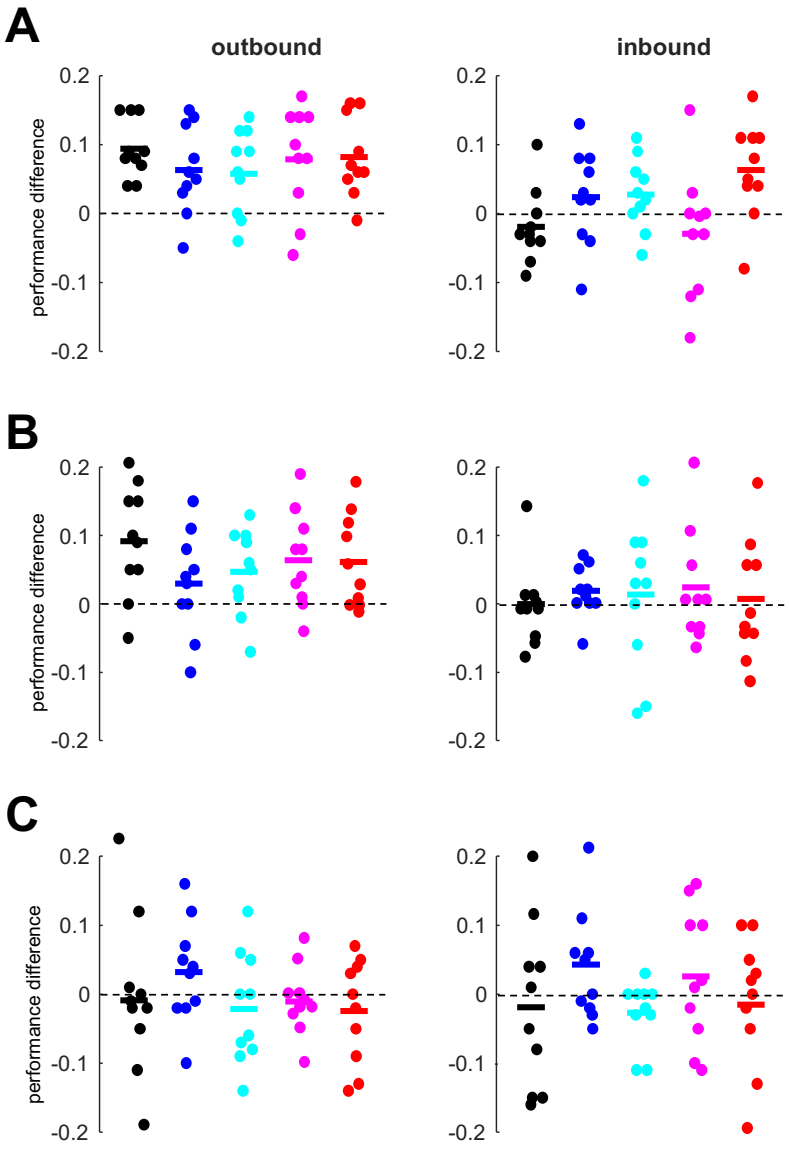

Fig. S8: Behavioral performance for individual animals and days
Each dot represents performance *difference* between the two M-maze sessions on each day, in either the outbound (left) or inbound (right) portions of the task. Each individual animal is plotted in a different color. Horizontal lines represent median for each animal. (**A)** Performance difference for the first cohort of rats (Figure S7A) between ripple prolongation sessions and no stimulation (days 1-5) or random stimulation sessions (days 6-10). (**B)** Performance difference for the second cohort of rats (Figure S7B) between ripple prolongation sessions and random stimulation sessions. (**C)** Performance difference for the third cohort of rats (Figure S7C) between random stimulation sessions and no stimulation sessions.

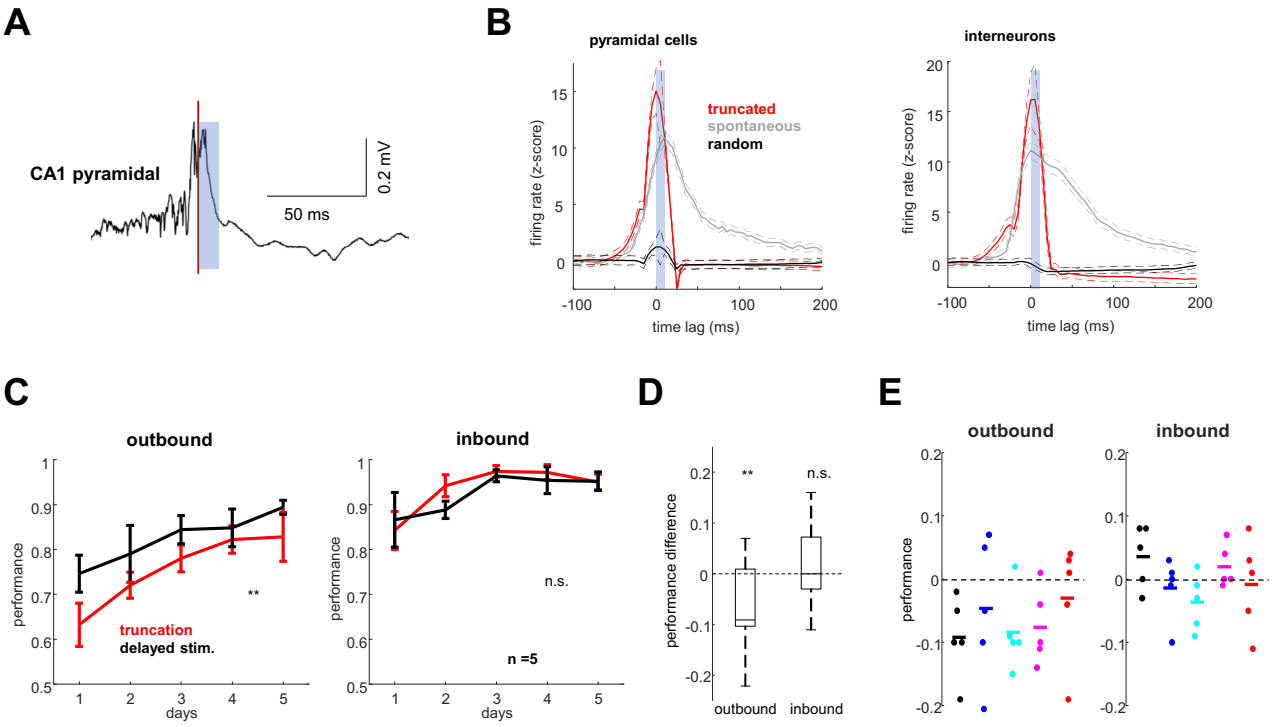

Fig. S9: SPW-R truncation impairs working memory.
(A), Example of a ripple truncation event. Red line indicates detection time and blue square shows light stimulation pulse. The strong, short stimulus (20 ms) induced a prolonged suppression of neuron firing. **(B)**, Firing rates of pyramidal cells and interneurons during spontaneous, truncated ripples and random stimulation (pyr: $P < 10^{-29}$ spontaneous versus truncated and $P < 10^{-14}$ spontaneous versus random n = 211. int: $P < 10^{-4}$ spontaneous versus truncated and $P < 10^{-11}$ spontaneous versus random n = 53; data from 5 rats (tested after 7 days of rest). 0 ms, onset of stimulation or peak of ripple power. **(C)**, Fraction of correct trials (mean ± SEM) in the M-maze task during outbound and inbound runs in ripple truncation and random stimulation sessions (n = 5 rats). $P < 0.01$, repeated measures ANOVA followed by Tuckey's post-hoc test ($P < 0.05$). **(D),** Performance differences for the same day and animal for ripple truncation versus random stimulation sessions. **$P < 0.01$, two-sided Wilcoxon signed rank test. (**E**) Performance difference between ripple truncation and random stimulation sessions of each day shown separately for each animal (different colors), in either the outbound (left) or inbound (right) portions of the task. Horizontal lines represent median for each animal.

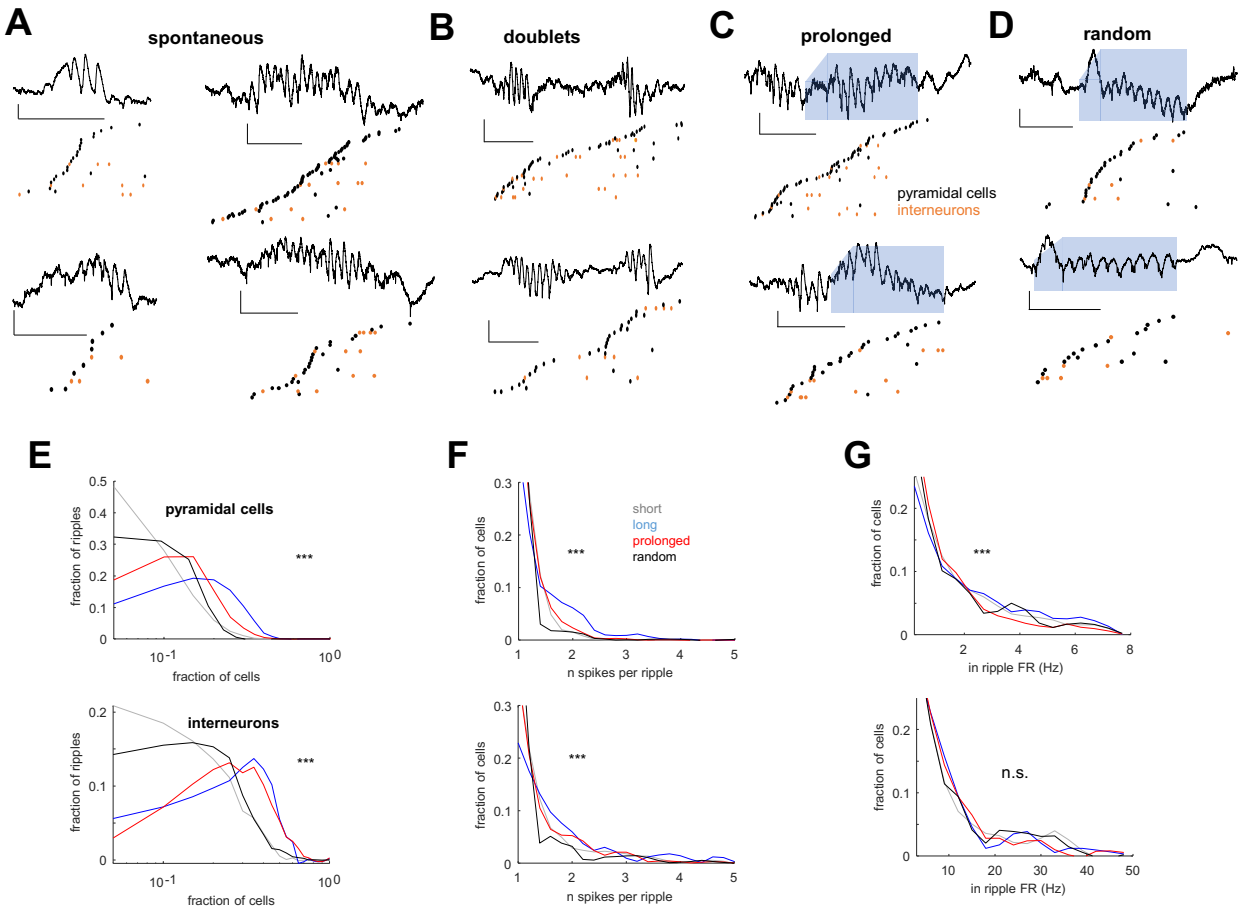

Fig. S10: Spike features in spontaneous, prolonged and random ripples.
(A-D), Examples of spike sequences in spontaneous short and spontaneous long ripples (**A**), spontaneous doublets (**B**), prolonged (**C**) and random ripples (**D**) from two different animals. Note that in the case of SPW-R doublets spiking sequences expand adjacent SPW-Rs, with most of the pyramidal cells firing during either the first or the second event but spikes of the same neurons rarely repeat. Black, pyramidal cells; red, interneurons. These panels illustrate our hypothesis than long SPW-Rs are formed due to the merging of shorter duration ripple events (Oliva et al., 2018). Vertical bar = 0.2 mV; horizontal bar = 50 ms. **(E-G)**, Characteristics of unit firing during spontaneous short and long SPW-Rs, prolonged and randomly induced ripples, shown separately for CA1 pyramidal cells (first row) and interneurons (second row). **(E)**, Fraction of all recorded neurons participating in each ripple type. **(F)**, Mean number of spikes of individual neurons emitted in each ripple. Note that the overwhelming majority of neurons fired only a single spike per ripple. **(G)**, Mean within-ripple firing rate per cell. $P < 0.001$, one-way ANOVA.

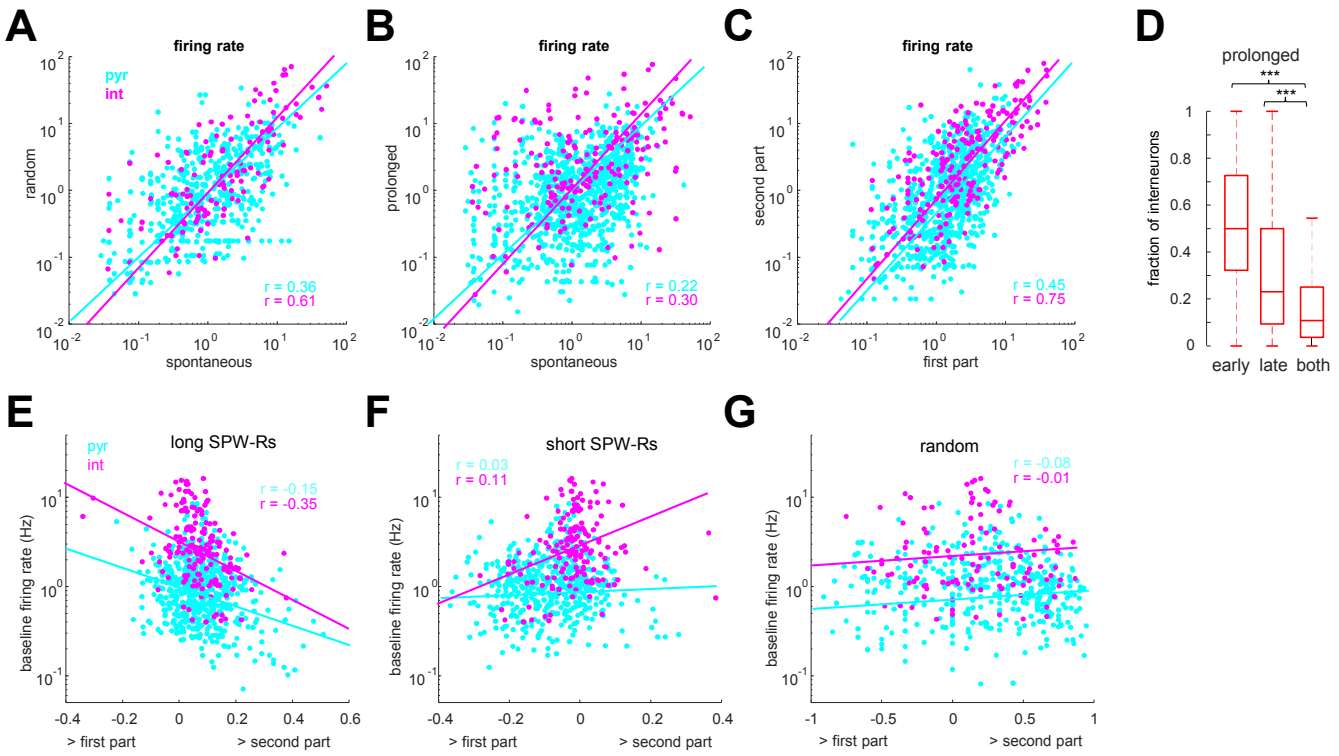

Fig. S11: Spike correlations in spontaneous, prolonged and random ripples
(A-B), Correlation of mean firing rates in ripples between spontaneous and random delay-induced ripples (**A;** $P < 10^{-22}$ / 10^{-15} for pyramidal cells and interneurons) and between spontaneous and prolonged ripples (**B;** $P < 10^{-12}$ / 10^{-5}). **(C)**, Correlation of firing rate in the spontaneous and stimulated parts of prolonged ripples ($P < 10^{-55}$ / 10^{-42}). **(D)**, Probability of firing in the early only, late only or both parts of prolonged ripples for all interneurons. (For pyramidal cells, see Figure 4c). *** $P < 0.001$ sign-rank test. **(E-G)**, Firing rate as a function of that neuron's probability of firing in the early versus late part of spontaneous long SPW-Rs (**E**, pyr r = -0.15, $P < 10^{-6}$; int r = -0.35, $P < 10^{-7}$), in short SPW-Rs (**F**, pyr r = 0.03, $P > 0.05$; int r = 0.11, $P > 0.05$) or randomly induced ripples (**G**, pyr r = 0.08, $P > 0.05$; int r = 0.01, $P > 0.05$) (for prolonged ripples, see Fig. 4E).

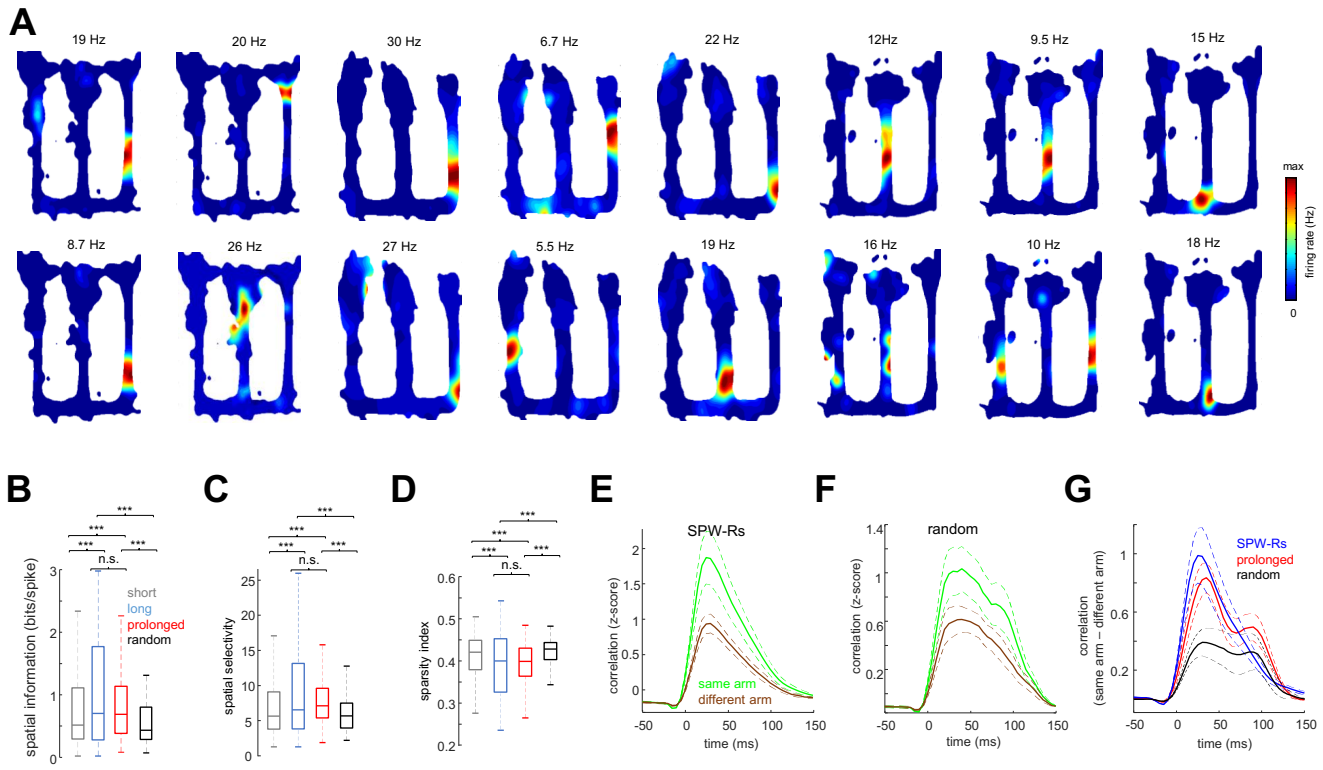

Fig. S12: Spatial coding features in in spontaneous, prolonged and random ripples.
(A), Examples of place cells in the M maze task. Upper row outbound travels and bottom row inbound. Numbers indicate peak firing rate of each map. **(B-D)**, Spatial coding properties of cells in spontaneous short, spontaneous long, prolonged and random ripples. b, Spatial information. **(C)**, Spatial selectivity. **(D)**, Sparsity index. ***, P < 0.001, rank-sum test. Note that spontaneous long and closed loop prolonged ripples are similar and both are different from spontaneous short and randomly induced ripples. **(E-F),** Cross-correlations between neurons z-scored firing rates in the first and second parts of spontaneous SPW-Rs (**E**) and randomly induced ones (**F**), shown separately for neurons representing the same or different side arms (P < 0.05 in both cases; signed-rank test). (**G**), Differences of spike cross-correlations between z-scored firing rates of early versus late part of the ripple between neurons representing the same or different side arms (P < 0.05 between spontaneous and prolonged ripples versus random ones, rank-sum test).

References and Notes

1. G. Buzsáki, Hippocampal sharp wave-ripple: A cognitive biomarker for episodic memory and planning. *Hippocampus* **25**, 1073–1188 (2015). doi:10.1002/hipo.22488 Medline

2. K. Diba, G. Buzsáki, Forward and reverse hippocampal place-cell sequences during ripples. *Nat. Neurosci.* **10**, 1241–1242 (2007). doi:10.1038/nn1961 Medline

3. D. J. Foster, M. A. Wilson, Reverse replay of behavioural sequences in hippocampal place cells during the awake state. *Nature* **440**, 680–683 (2006). doi:10.1038/nature04587 Medline

4. H. Xu, P. Baracskay, J. O'Neill, J. Csicsvari, Assembly responses of hippocampal CA1 place cells predict learned behavior in goal-directed spatial tasks on the radial eight-arm maze. *Neuron* **101**, 119–132.e4 (2019). doi:10.1016/j.neuron.2018.11.015 Medline

5. A. S. Gupta, M. A. A. van der Meer, D. S. Touretzky, A. D. Redish, Hippocampal replay is not a simple function of experience. *Neuron* **65**, 695–705 (2010). doi:10.1016/j.neuron.2010.01.034 Medline

6. S. Takahashi, Episodic-like memory trace in awake replay of hippocampal place cell activity sequences. *eLife* **4**, e08105 (2015). doi:10.7554/eLife.08105 Medline

7. S. P. Jadhav, C. Kemere, P. W. German, L. M. Frank, Awake hippocampal sharp-wave ripples support spatial memory. *Science* **336**, 1454–1458 (2012). doi:10.1126/science.1217230 Medline

8. D. Dupret, J. O'Neill, B. Pleydell-Bouverie, J. Csicsvari, The reorganization and reactivation of hippocampal maps predict spatial memory performance. *Nat. Neurosci.* **13**, 995–1002 (2010). doi:10.1038/nn.2599 Medline

9. T. J. Davidson, F. Kloosterman, M. A. Wilson, Hippocampal replay of extended experience. *Neuron* **63**, 497–507 (2009). doi:10.1016/j.neuron.2009.07.027 Medline

10. C. Drieu, R. Todorova, M. Zugaro, Nested sequences of hippocampal assemblies during behavior support subsequent sleep replay. *Science* **362**, 675–679 (2018). doi:10.1126/science.aat2952 Medline

11. B. E. Pfeiffer, D. J. Foster, Autoassociative dynamics in the generation of sequences of hippocampal place cells. *Science* **349**, 180–183 (2015). doi:10.1126/science.aaa9633 Medline

12. M. P. Karlsson, L. M. Frank, Awake replay of remote experiences in the hippocampus. *Nat. Neurosci.* **12**, 913–918 (2009). doi:10.1038/nn.2344 Medline

13. G. Dragoi, S. Tonegawa, Preplay of future place cell sequences by hippocampal cellular assemblies. *Nature* **469**, 397–401 (2011). doi:10.1038/nature09633 Medline

14. H. F. Ólafsdóttir, D. Bush, C. Barry, The role of hippocampal replay in memory and planning. *Curr. Biol.* **28**, R37–R50 (2018). doi:10.1016/j.cub.2017.10.073 Medline

15. M. A. Wilson, B. L. McNaughton, Reactivation of hippocampal ensemble memories during sleep. *Science* **265**, 676–679 (1994). doi:10.1126/science.8036517 Medline

16. G. Girardeau, K. Benchenane, S. I. Wiener, G. Buzsáki, M. B. Zugaro, Selective suppression of hippocampal ripples impairs spatial memory. *Nat. Neurosci.* **12**, 1222–1223 (2009). doi:10.1038/nn.2384 Medline

17. T. Nakashiba, D. L. Buhl, T. J. McHugh, S. Tonegawa, Hippocampal CA3 output is crucial for ripple-associated reactivation and consolidation of memory. *Neuron* **62**, 781–787 (2009). doi:10.1016/j.neuron.2009.05.013 Medline

18. E. Stark, L. Roux, R. Eichler, G. Buzsáki, Local generation of multineuronal spike sequences in the hippocampal CA1 region. *Proc. Natl. Acad. Sci. U.S.A.* **112**, 10521–10526 (2015). doi:10.1073/pnas.1508785112 Medline

19. J. O'Keefe, L. Nadel, *The Hippocampus as a Cognitive Map* (Oxford Univ. Press, 1978).

20. A. Oliva, A. Fernández-Ruiz, G. Buzsáki, A. Berényi, Role of hippocampal CA2 region in triggering sharp-wave ripples. *Neuron* **91**, 1342–1355 (2016). doi:10.1016/j.neuron.2016.08.008 Medline

21. A. Oliva, A. Fernández-Ruiz, E. Fermino de Oliveira, G. Buzsáki, Origin of gamma frequency power during hippocampal sharp-wave ripples. *Cell Rep.* **25**, 1693–1700.e4 (2018). doi:10.1016/j.celrep.2018.10.066 Medline

22. S. M. Kim, L. M. Frank, Hippocampal lesions impair rapid learning of a continuous spatial alternation task. *PLOS ONE* **4**, e5494 (2009). doi:10.1371/journal.pone.0005494 Medline

23. E. Pastalkova, V. Itskov, A. Amarasingham, G. Buzsáki, Internally generated cell assembly sequences in the rat hippocampus. *Science* **321**, 1322–1327 (2008). doi:10.1126/science.1159775 Medline

24. M. Tsodyks, T. Kenet, A. Grinvald, A. Arieli, Linking spontaneous activity of single cortical neurons and the underlying functional architecture. *Science* **286**, 1943–1946 (1999). doi:10.1126/science.286.5446.1943 Medline

25. N. Maingret, G. Girardeau, R. Todorova, M. Goutierre, M. Zugaro, Hippocampo-cortical coupling mediates memory consolidation during sleep. *Nat. Neurosci.* **19**, 959–964 (2016). doi:10.1038/nn.4304 Medline

26. R. M. Memmesheimer, Quantitative prediction of intermittent high-frequency oscillations in neural networks with supralinear dendritic interactions. *Proc. Natl. Acad. Sci. U.S.A.* **107**, 11092–11097 (2010). doi:10.1073/pnas.0909615107 Medline

27. M. F. Carr, M. P. Karlsson, L. M. Frank, Transient slow gamma synchrony underlies hippocampal memory replay. *Neuron* **75**, 700–713 (2012). doi:10.1016/j.neuron.2012.06.014 Medline

28. J. Yamamoto, S. Tonegawa, Direct medial entorhinal cortex input to hippocampal CA1 is crucial for extended quiet awake replay. *Neuron* **96**, 217–227.e4 (2017). doi:10.1016/j.neuron.2017.09.017 Medline

29. J. O'Neill, C. N. Boccara, F. Stella, P. Schoenenberger, J. Csicsvari, Superficial layers of the medial entorhinal cortex replay independently of the hippocampus. *Science* **355**, 184–188 (2017). doi:10.1126/science.aag2787 Medline

30. S. P. Jadhav, G. Rothschild, D. K. Roumis, L. M. Frank, Coordinated excitation and inhibition of prefrontal ensembles during awake hippocampal sharp-wave ripple events. *Neuron* **90**, 113–127 (2016). doi:10.1016/j.neuron.2016.02.010 Medline

31. A. Fernández-Ruiz, A. Oliva, G. A. Nagy, A. P. Maurer, A. Berényi, G. Buzsáki, Entorhinal-CA3 dual-input control of spike timing in the hippocampus by theta-gamma coupling. *Neuron* **93**, 1213–1226.e5 (2017). doi:10.1016/j.neuron.2017.02.017 Medline

32. A. Ylinen, A. Bragin, Z. Nádasdy, G. Jandó, I. Szabó, A. Sik, G. Buzsáki, Sharp wave-associated high-frequency oscillation (200 Hz) in the intact hippocampus: Network and intracellular mechanisms. *J. Neurosci.* **15**, 30–46 (1995). doi:10.1523/JNEUROSCI.15-01-00030.1995 Medline

33. A. Fernández-Ruiz, V. A. Makarov, N. Benito, O. Herreras, Schaffer-specific local field potentials reflect discrete excitatory events at gamma frequency that may fire postsynaptic hippocampal CA1 units. *J. Neurosci.* **32**, 5165–5176 (2012). doi:10.1523/JNEUROSCI.4499-11.2012 Medline

34. A. Fernández-Ruiz, S. Muñoz, M. Sancho, J. Makarova, V. A. Makarov, O. Herreras, Cytoarchitectonic and dynamic origins of giant positive local field potentials in the dentate gyrus. *J. Neurosci.* **33**, 15518–15532 (2013). doi:10.1523/JNEUROSCI.0338-13.2013 Medline

35. E. W. Schomburg, A. Fernández-Ruiz, K. Mizuseki, A. Berényi, C. A. Anastassiou, C. Koch, G. Buzsáki, Theta phase segregation of input-specific gamma patterns in entorhinal-hippocampal networks. *Neuron* **84**, 470–485 (2014). doi:10.1016/j.neuron.2014.08.051 Medline

36. E. Stark, L. Roux, R. Eichler, Y. Senzai, S. Royer, G. Buzsáki, Pyramidal cell-interneuron interactions underlie hippocampal ripple oscillations. *Neuron* **83**, 467–480 (2014). doi:10.1016/j.neuron.2014.06.023 Medline

37. A. D. Grosmark, G. Buzsáki, Diversity in neural firing dynamics supports both rigid and learned hippocampal sequences. *Science* **351**, 1440–1443 (2016). doi:10.1126/science.aad1935 Medline

38. C. Rossant, S. N. Kadir, D. F. M. Goodman, J. Schulman, M. L. D. Hunter, A. B. Saleem, A. Grosmark, M. Belluscio, G. H. Denfield, A. S. Ecker, A. S. Tolias, S. Solomon, G. Buzsáki, M. Carandini, K. D. Harris, Spike sorting for large, dense electrode arrays. *Nat. Neurosci.* **19**, 634–641 (2016). doi:10.1038/nn.4268 Medline

39. K. Mizuseki, A. Sirota, E. Pastalkova, G. Buzsáki, Theta oscillations provide temporal windows for local circuit computation in the entorhinal-hippocampal loop. *Neuron* **64**, 267–280 (2009). doi:10.1016/j.neuron.2009.08.037 Medline

40. M. Pachitariu, N. A. Steinmetz, S. N. Kadir, M. Carandini, K. D. Harris, "Fast and accurate spike sorting of high-channel count probes with KiloSort," in *Advances in Neural Information Processing Systems 29*, D. D. Lee, M. Sugiyama, I. Guyon, R. Garnett, Eds. (NIPS, 2016), pp. 4448–4456.